Renewable Energy 51 (2013) 141–152

Contents lists available at SciVerse ScienceDirect

Renewable Energy

journal homepage: www.elsevier.com/locate/renene

Flow control for VATT by fixed and oscillating flap

Qing Xiao*, Wendi Liu, Atilla Incecik

Department of Naval Architecture and Marine Engineering, University of Strathclyde, Glasgow G4 0LZ, UK

ARTICLE INFO

Article history:
Received 7 March 2012
Accepted 23 September 2012
Available online 17 October 2012

Keywords:
Vertical axis tidal turbine
Computational fluid dynamics
Flap

ABSTRACT

The present study is aimed to explore the potential to improve Vertical Axis Tidal Turbine (VATT) energy harnessing efficiency by using modified blades with fixed and oscillating flap. The fixed flap concept is borrowed from its application in aerodynamics area for reaching a high lift force at low flying speed. Oscillating flap is motivated by our relevant biomimetic studies on the flapping wing propulsion or energy extraction. Present investigation is concentrated on a VATT with NACA 0018 profile blade as its baseline turbine. Numerical simulations are carried out by solving incompressible Unsteady Navier–Stokes equations at turbulence flow condition. Computed results show that under certain optimal flap geometry and flow conditions, turbine power coefficient reaches 28% enhancement as compared to the conventional blade turbine. Detailed analysis on the flow structure demonstrates that this is related to the effective flow separation suppression and vortex control by applying a fixed and oscillating flap.

1. Introduction

In recent decades, the huge increase in global demand for energy by the technology and industry boom has brought renewable energy back to the top of the world's agenda. Among various ocean renewable energies, tidal energy has its distinct superiorities over other types of ocean energy. It has much less sensitivity to the climate change and is predictable in both space and time domains. Tidal turbine is gradually becoming one of the most efficient devices which transform tidal energy into mechanical power [1].

Present study is focused on an H-shaped lift force driven Vertical Axis Tidal Turbine (VATT). In comparison with the horizontal axis turbine and drag force driven turbine, H-shaped turbine has many advantages, such as its simple blade design, its ability to function from all current flow directions and it's non-sensitivity to water depth. Nonetheless, the efficiency of existing H-shaped VATT is still relative low as compared to the horizontal axis turbine. It thus exists the necessity and huge potential benefits in carrying out further research in order to enhance VATT efficiency via various mechanical and control methods [2,3].

There are many factors which influence VATT energy conversion efficiency. Assessing from the fluid analysis perspective, dynamic stall is one of the key factors that debilitates the devices efficiency. Stall occurs due to flow separation when turbine blade rotates to a position at large angle of attack. Once that happens, the blade lift force is adversely affected and drops significantly, leading to the overall reduced energy extraction efficiency. This is obviously very undesirable for the lift force driven VATT which is topic of the stated research. In aerodynamics applications, to delay the aero-wing stall by eliminating or delaying the flow separation, various flow control approaches have been explored. Modifying a full aircraft wing with a slot and a fixed flap near aft wing, as depicted in Fig. 1(b), is found to be one of the most effective techniques to control the air flow across the wing attaching to the wing surface [4–11].

The idea of using a fixed flap with slot for aerodynamics flow control was initially developed by Page [4] and Glauert [5] in the 1920s, aiming to achieve a large lift force for a wing at a relatively low flying speed. Weyl [6] also contributed significantly to the development of split flap during 1915–1920. In 1927, Fowler flap was invented by Fowler [7] and subsequently tested in NASA wind-tunnel [8]. Experimental measurements proved that with the use of Fowler flap, the wing maximum lift coefficient increases to 3.17 [9]. Since then, various other types of flaps have been developed such as plain flap, junkers flap, gouge flap etc. [10,11]. Recently, the slotted aero-wing with flap has been widely adopted in the aircraft design by several famous aircraft companies such as Boeing, Airbus and Douglas to improve the aircraft taking off performance when a high lift is desired. Apart from the single slot technique, multiple slots method is also used by the modern aircraft designers in order to boost the benefits of slot.

For a VATT, the blade angle of attack usually varies over a wide range when the blade rotates around a rotor, thus large angle of attack and flow separation are inevitable for the traditional turbine

* Corresponding author. Tel.: +44 141 5484779.
E-mail address: qing.xiao@strath.ac.uk (Q. Xiao).

0960-1481/$ – see front matter © 2012 Elsevier Ltd. All rights reserved.
http://dx.doi.org/10.1016/j.renene.2012.09.021

Nomenclature

c	Blade chord (m)
C_l	Lift coefficient
C_m	Moment coefficient
C_p	Power coefficient
D	Turbine diameter (m)
L	Slot location (m)
L_{if}	Lift force (N)
M	Moment (N m)
n	Frequency ratio
P	Power (W)
P_{re}	Pressure (Pa)
R	Turbine radius (m)
T_{flap}	Oscillating flap revolution (s)
T_{turb}	Turbine revolution (s)
U	Velocity of incoming flow (m/s)
w	Slot width (m)
β	Flap angle (deg)
β_0	Oscillating amplitude (deg)
γ	Slot angle (deg)
θ	Turbine azimuthal angle (deg)
λ	Turbine blade tip speed ratio
ρ	fluid density (kg/m^3)
ω	Turbine angular velocity (rad/s)
ω_f	Oscillating flap angular velocity (rad/s)

constituting of full blades, as shown in Fig. 1(a). The concept of slotted blade with flap, which enjoys considerable success in the aerodynamics field, is an ideal solution for the mentioned issues. By adding a slot near the trailing edge of turbine blade, small amount of water stream is forced to pass through the slot from high pressure region to low pressure region. The large momentum associated with the high pressure stream imparts its energy into the boundary layer near the upper surface of blade, resulting in the developed boundary layer on the base blade breakdown and forming a new boundary layer on the flap part. Such method is believed to reduce the near boundary turbulence intensity effectively and delay the boundary layer detachment in the vicinity of blade trailing edge, and consequently reducing blade lift force losses and improving turbine efficiency.

Inspired by the vortex control mechanism, utilized by some aero-/aqua- animals to improve their propulsion performance via their fins or tails flapping motion [12,13], slotted blade with *oscillating* flap is developed and investigated in the present study. The oscillating flap is designed to move periodically around a pitching axis as shown in Fig. 1(c). Distinctive from a fixed flap, the use of an oscillating flap not only controls the near boundary layer fluid flow, but also regulates the vortex interaction in the wake between each blade. For multiple-blade turbine as studied in this paper, the flow analysis focusing on the blade wake vortex interference is therefore crucial for enhancing the overall turbine performance.

In this paper, a numerical investigation is carried out with the main objective to explore the potential for enhancing VATT energy extraction efficiency by using fixed and oscillating flap blade. As far as the authors are aware of, applying oscillating flap concept on VATT as a flow control tool is generally a new area of development, and no substantial research has been conducted as of yet.

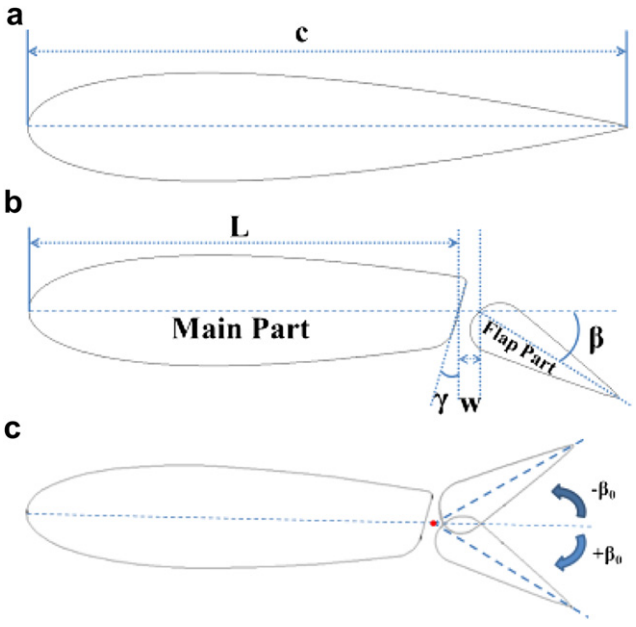

Fig. 1. Three different blades in present study (a) Full blade; (b) Slotted blade with fixed flap; (c) Slotted blade with oscillating flap.

2. Numerical method

2.1. Description of problem

The simulated turbine model, plotted in Fig. 2, is based on a real marine current turbine, currently operates at WANXIANG II station in China [14]. Detailed geometry parameters and operating conditions are summarized in Table 1. To simplify the problem, the blade is assumed to be infinitely long in span-wise direction, and therefore the two-dimensional modeling is conducted. The Reynolds number is defined as $Re = R\omega c/\nu$, where R is the radius of turbine, c is the chord length, ω is the rotational angular speed and ν is the viscosity. The Reynolds number used in the present simulation is set as 4.7×10^5 which is identical to real operating conditions. The turbine azimuthal angle (θ) is defined as the angle which sweeps from the positive X-axis to the line connecting origin to the blade mass center as shown in Fig. 2.

Three different types of turbine blades are investigated as shown in Fig. 1(a) to (c) for the full blade, slotted blade with a fixed

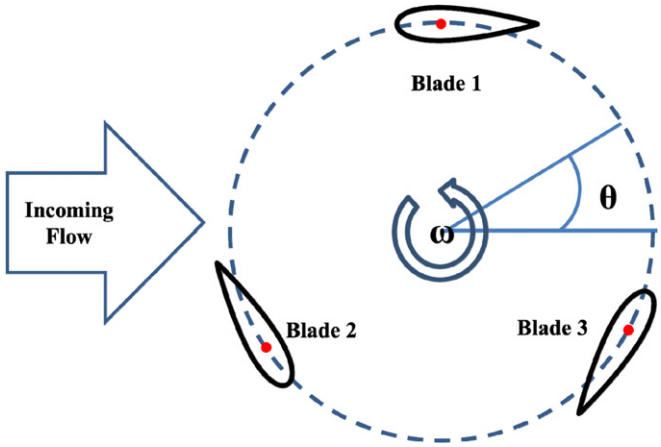

Fig. 2. Schematic diagram of flow configuration.

Table 1
Operating conditions of WANXIANG II power station (From Castelli et al. (2011) [15]).

Blade profile	NACA 0018	
Rotor diameter	2.5	m
Number of blades	3	
Blade length	5	m
Blade chord	0.3	m
Solidity	0.72	m
Rated power	40	KW
Stream speed	1.6	m/s
Rotational speed	1.2672	rad/s
Reynolds number	4.7×10^5	

flap and slotted blade with an oscillating flap. For a fixed flap blade, a slot is cut at a distance L away from blade leading edge with a slot angle of γ° and a slot width of w. The slot divides the full blade into two parts, i.e. main blade part and flap blade part. The angle between the flap center line and the main part center line is defined as flap angle β. For an oscillating flap, the flap rotates with its axis at the center of gap between main and flap parts with the following specified motion equation as

$$\omega_f = \beta_0 \sin\left(n\omega t + \frac{\pi}{2}\right) \tag{1}$$

where β_0 represents the amplitude of flap and ω_f is the rotational angular velocity of oscillating flap. To quantify the oscillating flapping motion relative to the turbine rotational motion, one parameter 'n' is introduced, which is defined as below

$$n = T_{\text{turb}}/T_{\text{flap}} \tag{2}$$

where T_{turb} and T_{flap} are revolution of turbine and oscillating flap, respectively.

2.2. Computational methodology

The present simulation is based on solving Unsteady Reynolds-averaged Navier–Stokes equations (URANS) by using the commercial CFD package FLUENT 12.1. The governing equations for unsteady incompressible flow associated with mass and moment conservation are as follows

$$\rho \frac{\partial \vec{v}}{\partial t} = \vec{F} - \nabla \cdot p + \mu \nabla^2 \vec{v} \tag{3}$$

and

$$\nabla \cdot \vec{v} = 0 \tag{4}$$

where ρ is the density of fluid, $\vec{v}$ is the vector of velocity, t is the instantaneous time, $\vec{F}$ is the body force on the fluid, p is the pressure and μ is the dynamic viscosity.

The modeling is assumed to be two-dimensional within an isothermal fluid domain. Second order finite volume solver is adopted along with the SIMPLEC algorithm for pressure-velocity coupling. To model the turbulence, various turbulence models are tested and the results indicate that the realizable k–ε turbulent model is the most accurate model for the present problem (shown later). To well capture the near wall boundary layer while using reasonable mesh points, the standard wall function is used along with k–ε turbulent model. The detailed turbulent model is governed by the following two equations as

$$\frac{\partial}{\partial t}(\rho k) + \frac{\partial}{\partial x_i}(\rho k u_i) = \frac{\partial}{\partial x_i}\left[\left(\mu + \frac{\mu_t}{\sigma_k}\right)\frac{\partial k}{\partial x_j}\right] + G_k + G_b - \rho_\varepsilon \varepsilon - Y_M + S_k \tag{5}$$

and

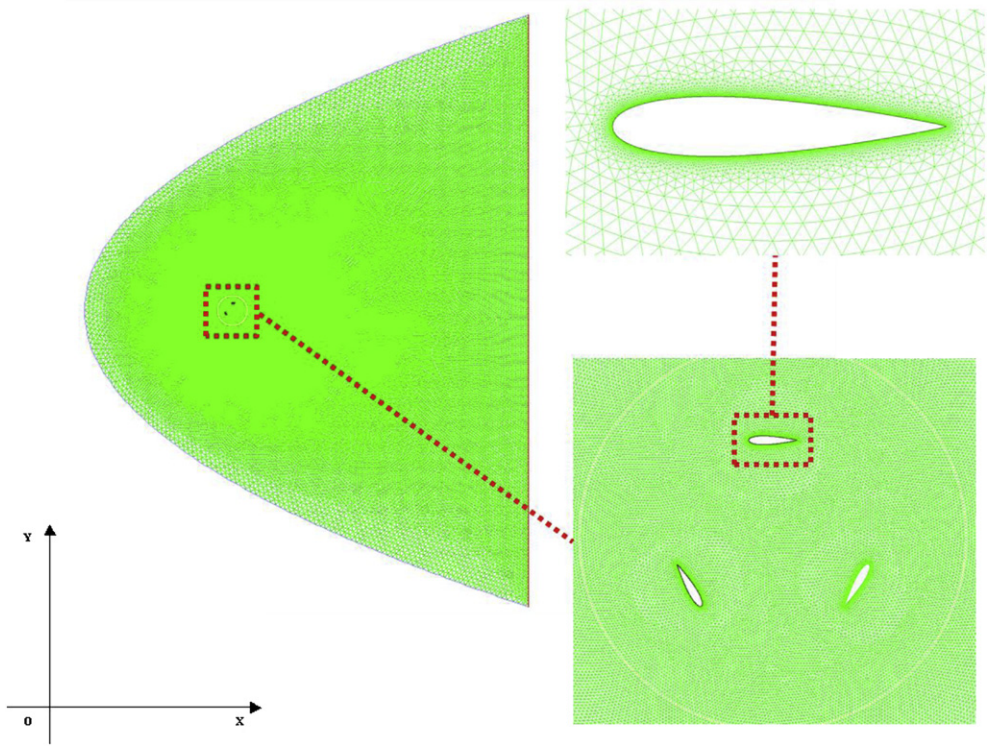

Fig. 3. Computational domain and mesh distribution.

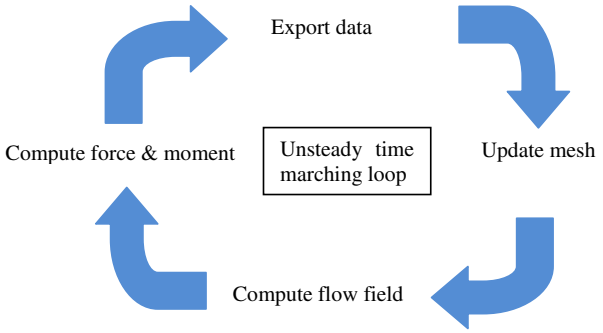

Fig. 4. Schematic diagram for unsteady time marching.

$$\frac{\partial}{\partial t}(\rho\varepsilon)+\frac{\partial}{\partial x_i}(\rho\varepsilon u_i)=\frac{\partial}{\partial x_i}\left[\left(\mu+\frac{\mu_t}{\sigma_\varepsilon}\right)\frac{\partial\varepsilon}{\partial x_j}\right]+C_{1\varepsilon}\frac{\varepsilon}{k}(G_k+C_{3\varepsilon}G_b)-C_{2\varepsilon}\rho\frac{\varepsilon^2}{k}+S_\varepsilon \quad (6)$$

where k is the turbulent kinetic energy and ε is the dissipation rate of kinetic energy. G_k is the generation of turbulent kinetic energy due to the mean velocity gradients; G_b is the generation of turbulent kinetic energy due to the buoyancy; Y_M is the contribution of the fluctuating dilatation in compressible turbulence to the overall dissipation rate; S is the source and σ is the Prandtl number.

The computational domain and mesh is shown in Fig. 3. The turbine is set 9D (turbine diameter) away from the inlet boundary and 20D away from the outlet boundary. An uniform constant velocity in x direction is applied as the incoming flow for inlet boundary condition as $u=U_\infty$, $v=0$ and $\partial p/\partial x=0$. Pressure outlet with $\partial p/\partial n=0$ is adopted for the outlet boundary. For ease of mesh generation and also due to the dynamic mesh method imbedded in FLUENT is adopted for handling the oscillating motion of blade flap, an unstructured grid is constructed within the entire computational domain, while a structured grid is used in the near wall boundary layer around the blade.

The unsteady solution loop within one unsteady time-step is shown in Fig. 4. As shown, the macro CG motion along with User Defined Function (UDF) are adopted to control the sliding mesh for turbine rotor and oscillating flap motion. To maintain the mesh twist at a low level, the spring smoothing and re-meshing function is used. The overall flow field problem is solved based on the inertial frame. The instantaneous force and moment of all blades are calculated using UDF and saved at regular time intervals.

2.3. Key parameters

Several key parameters which quantify the turbine performance include the power coefficient C_p, the blade moment coefficient C_m, the blade tip speed ratio λ and the blade lift coefficient C_L. Detailed definitions are described below.

Table 2
Main geometry and flow conditions for Darrieus wind turbine (From Castelli et al., 2011 [15]).

Blade profile	NACA 0021	
Rotor diameter	1.03	m
Number of blades	3	
Blade length	1.4564	m
Blade chord	0.0858	m
Solidity	0.5	m
Stream speed	9	m/s
Reynolds number	7.5×10^5	

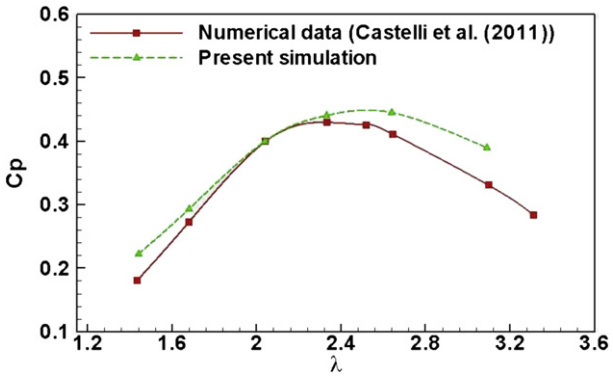

Fig. 5. Time-averaged power coefficient variation with tip speed ratio (Comparison with Castelli et al. (2011) [15]).

The power coefficient C_p is determined by

$$C_p=\frac{P}{\frac{1}{2}\rho U^3 D} \quad (7)$$

and

$$P=\sum_i M_i\cdot\omega \quad (8)$$

where P is the power generated by turbine defined in Equation (8), ω is the turbine angular velocity, M is the blade moment relative to the turbine center, ρ is the fluid density, U is the velocity of the incoming flow and D is the turbine diameter.

The blade moment coefficient C_m is defined as

$$C_m=\frac{M}{\frac{1}{2}\rho U^2 D^2} \quad (9)$$

and the pressure coefficient is determined by

$$\text{Pressure coefficient}=\frac{P_{re}}{\frac{1}{2}\rho U^2} \quad (10)$$

where P_{re} is the total pressure on the blade.

The turbine blade tip speed ratio is defined by

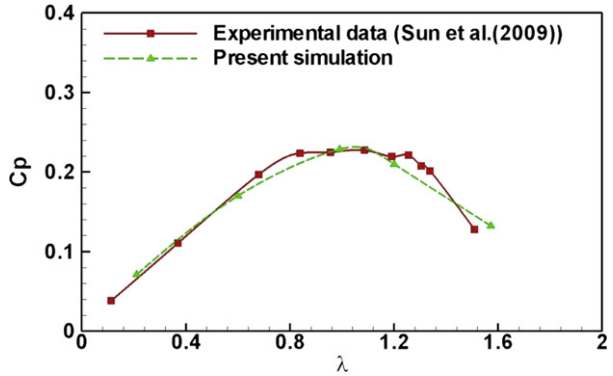

Fig. 6. Time-averaged power coefficient variation with tip speed ratio (Comparison with Sun et al. (2009) [14]).

Table 3
Mesh dependence test (Error is relative to experimental C_p of 0.442).

Mesh density	First grid point near wall	Number of cells in the domain	C_p	Error	Running time
Coarse	0.03	112,626	0.314	28.9%	4 h
Medium	0.01	383,511	0.427	3.4%	10 h
Fine	0.005	785,056	0.446	−0.9%	36 h

$$\lambda = \frac{\omega R}{U} \tag{11}$$

where R is turbine radius.

The blade lift coefficient is defined as

$$C_l = \frac{L_{if}}{\frac{1}{2}\rho U^2 c} \tag{12}$$

where L_{if} is the lift force.

3. Results and discussions

3.1. Model validation

The computational methodology developed in present study is verified against a Darrieus wind turbine and a passive pitch control VATT where either the numerical or experimental data are available [14,15].

The main geometry and flow conditions for Darrieus wind turbine is summarized in Table 2. The comparison of present computed time-mean power coefficient against tip speed ratio (λ) with Castelli et al. [15] simulation results are shown in Fig. 5. It can be seen that the predicted power coefficient agrees well with Castell et al's results for tip speed ratio between 1.8 and 2.2. However, some discrepancies appear between two results for λ larger than 2.4 or less than 1.8. This could be due to the occurrence of strong flow separation at large speed ratios and thus the simulation becomes more sensitive to the computational mesh and turbulence model adopted. For $\lambda < 1.8$, the different mesh structure near the blade wall in two studies might be the cause of such disagreement, where the unstructured mesh is used in Castelli et al with the relative coarse grid points while a fine structured mesh is adopted in the present investigation.

Flow of a passive pitch control VATT (Sun et al. [14]) is also simulated as second validation case. The main reason to select such a relatively complicated case as a part of our validation is due to the available experimental data. In addition, the present research is focused on a VATT with an active controlled oscillating flap blade, and this is further expected to extend to our near future study on a passive controlled flap. Successful validation on our developed model with Sun et al.'s case will benefit for our future study. Fig. 6 shows the time-averaged power coefficient variation with tip speed ratio for present simulation and the experimental data from Sun et al. [14]. A high level of good agreement between the present two-dimensional simulation results and their experimental data, based on the blade aspect ratio of 6.0, is clearly seen from Fig. 6 indicating the accuracy of present numerical methods. The spikes that are presented in the experimental data between $\lambda = 0.8$ and 1.3 are attributed to unavoidable measuring errors.

Apart from above two validations, the unsteady time-step, mesh independence and turbulence model testing are performed before the detailed investigation. Grid dependence test is carried out for a full blade turbine at a time-step of 0.5deg/step with two equation Realizable k–ε turbulence model at $\lambda = 0.99$. The time-mean power coefficients are compared in Table 3 along with detailed mesh information. Fig. 7 compares the instantaneous blade moment coefficient (C_m) for three sets of grids. Based on these comparisons, there is no significant difference between the medium and fine grid, and therefore for simplicity purposes, all simulations below are computed by medium grid.

Table 4
Unsteady time-step size and turbulent model test (error is relative to experimental C_p of 0.442).

Turbulent model	Time-step	C_p	Error	Running time
Reynolds stress (5 eqn)	0.5°/step	0.411	7.0%	12 h
SST k–ω	0.5°/step	0.329	25.6%	12 h
Realizable k–ε	0.5°/step	0.427	3.4%	12 h
Realizable k–ε	0.2°/step	0.446	−0.9%	36 h
Realizable k–ε	0.1°/step	0.454	−2.7%	84 h

Table 5
Comparison of key performance parameters for three different turbines ($\lambda = 1.572$; slotted parameters: $\gamma = 30°$, $w = 0.03c$ and $L = 0.7c$; oscillating flap amplitude: $\beta_0 = 30°$).

	Time-mean C_p	Max. C_m	Max. C_l	Separation point
Full blade	0.222	0.153	0.181	0.7c
Slotted blade with fixed flap	0.421	0.293	0.445	0.967c
Slotted blade with oscillating flap	0.514	0.380	0.580	0.950c

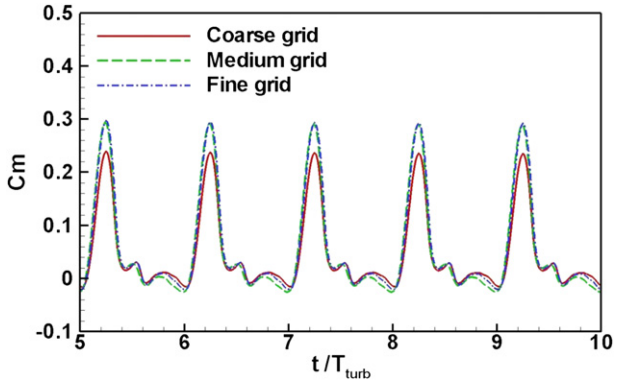

Fig. 7. Instantaneous blade moment coefficient variation with instantaneous time (grid dependence test).

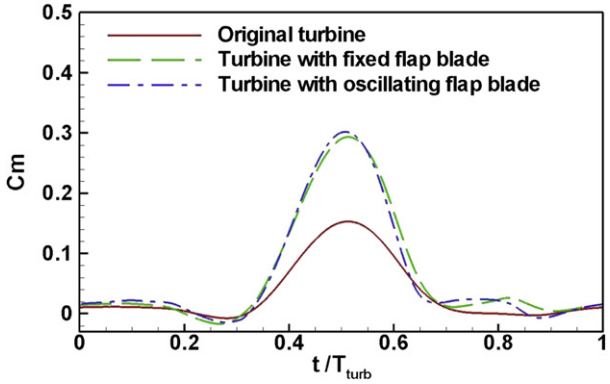

Fig. 8. Comparison of instantaneous blade moment coefficient against time for three different blade turbines ($\lambda = 1.572$). For slotted blade, $\gamma = 30°$, $w = 0.03c$ and $L = 0.7c$; For oscillating blade, $\beta_0 = 30°$.

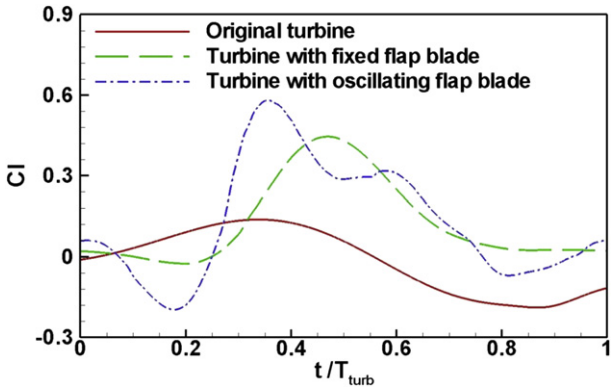

Fig. 9. Comparison of instantaneous blade lift coefficient against time for three different blade turbines ($\lambda = 1.572$). For slotted blade, $\gamma = 30°$, $w = 0.03c$ and $L = 0.7c$; For oscillating blade, $\beta_0 = 30°$.

The effect of turbulence modeling and unsteady time-step on the computed results are performed for an oscillating flap blade turbine at $\gamma = 30°$; $w = 0.03c$; $L = 0.7c$; $\beta_0 = 15°$ and $n = 1.5$. Predicted time-mean C_p is listed in Table 4. As can be seen from this table, there are no obvious difference on power coefficient with reducing the time-step size. Considering the significant increased computational time with small time-step, 0.5deg/step is used in the present simulations. As to the various turbulence models tested, realizable $k-\varepsilon$ model obtains the closest result to validated case among three turbulence models tested.

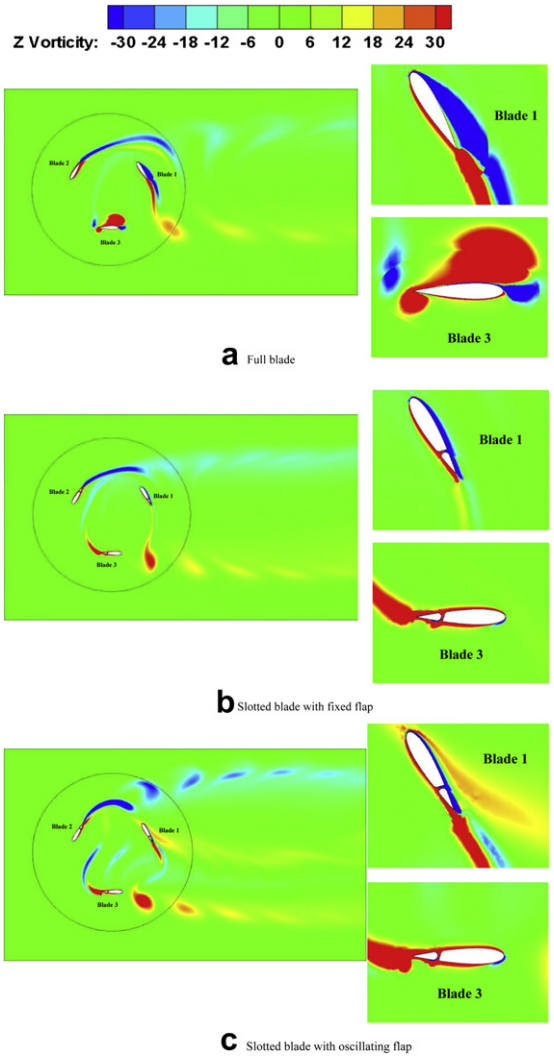

Fig. 10. Comparison of vortex contour at instantaneous time of $t/T_{turb} = 5/12$ for three different blades with $\lambda = 1.572$ (a) full blade; (b) fixed flap blade $\gamma = 30°$; $w = 0.03c$; $L = 0.7c$; (c) oscillating flap blade $\gamma = 30°$; $w = 0.03c$; $L = 0.7c$ and $\beta_0 = 30°$.

3.2. Mechanism of flow control by fixed and oscillating flap

Before a systematic parametric study is performed on a VATT with the fixed and oscillating blade, the study on a potential efficiency improvement by the properly flow control mechanism through the use of fixed and oscillating flap is carefully conducted under several flow and turbine geometric conditions. A specific case, with tip speed ratio $\lambda = 1.572$, is used to present our results below. Detailed discussion on the power coefficient, instantaneous momentum coefficient, lift coefficient and vortex contours are presented and compared among three different turbines, i.e. full blade turbine, fixed flap turbine with $\gamma = 30°$, $w = 0.03c$ and $L = 0.7c$ and oscillating flap turbine with $\gamma = 30°$, $w = 0.03c$ and $L = 0.7c$ and oscillating amplitude of $\beta_0 = 30°$.

The time-mean power coefficient (C_p), maximum momentum coefficient (C_m), maximum lift coefficient (C_l) and blade surface flow separation point are summarized in Table 5 for the comparison among three turbines tested. It is seen from this table that, the turbine with oscillating flap reaches a maximum time-mean power coefficient among three turbines, which is about as much as 2.31 times of full blade and 1.22 times of fixed flap blade. Examinations on the instantaneous Cm and Cl variation in one revolution (shown in Figs. 8 and 9) indicate that this is attributed to the increased C_m

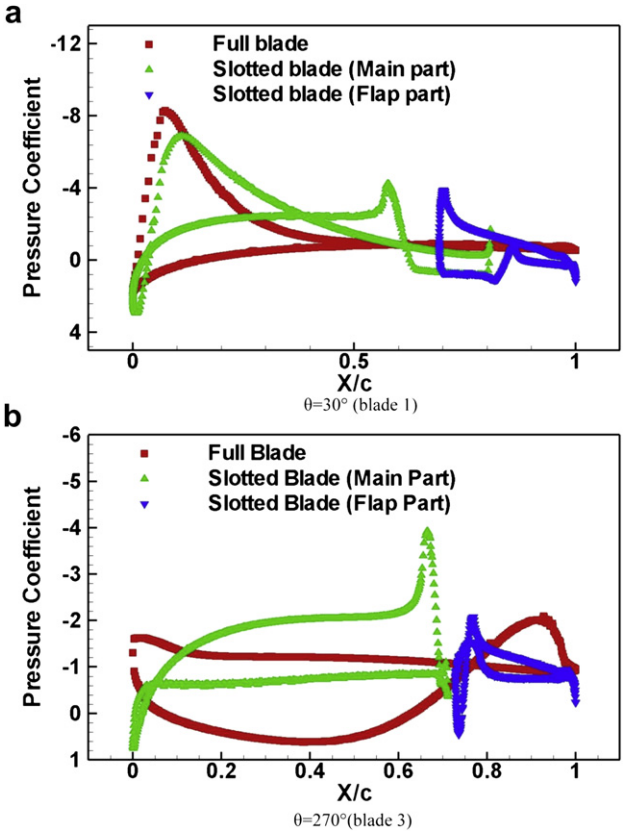

Fig. 11. Blade surface pressure coefficient distribution at $\lambda = 1.572$ (a) $\theta = 30°$ (blade 1); (b) $\theta = 270°$(blade 3).

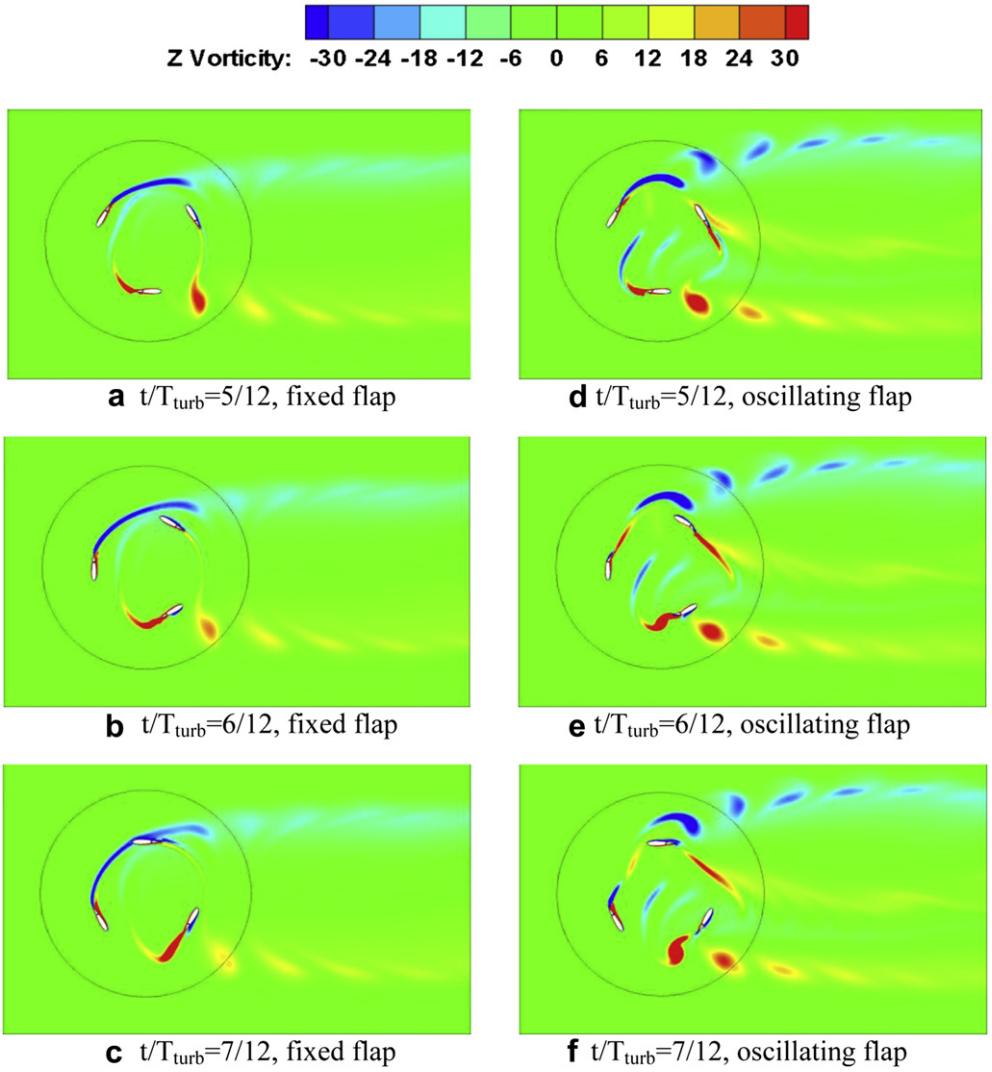

Fig. 12. Comparison of vortex contour within one revolution for slotted fixed and oscillating flap at $\lambda = 1.572$ with $\gamma = 30^{\circ}$; $w = 0.03c$; $L = 0.7c$. (a) $t/T_{turb} = 5/12$, fixed flap; (b) $t/T_{turb} = 6/12$ fixed flap (c) $t/T_{turb} = 7/12$, fixed flap; (d) $t/T_{turb} = 5/12$, oscillating flap; (e) $t/T_{turb} = 6/12$, oscillating flap; (f) $t/T_{turb} = 7/12$, oscillating flap. For oscillating flap, the amplitude is $\beta_0 = 30^{\circ}$.

and C_l peak values at instantaneous time of 0.5Ttub. It is obvious from the fact that for a lift-driven turbine, increasing blade lift force can lead to the enhancement of overall turbine torque and energy extraction.

The impact of slotted blade with a fixed or oscillating flap on the flow structure can be also seen from the vortex contour plots in Fig. 10(a)–(c). With a full blade, the development of flow boundary layer along the blades at azimuthal angle of 30°, 150° and 270° (blade 1–3) are clearly seen. At azimuthal angle of 30° (blade 1), the boundary layer detaches from the blade at about half of the chord length. When the blade rotates to 270° position (blade 3), several large vortices are observed due to the strong flow separation at large angle of attack, leading to the dynamic stall of turbine and as a consequence a diminish in energy harnessing efficiency. In contrast, the vortices contour associated with the slotted turbine blade, plotted in Fig. 10(b), shows the attached flow along the blade at azimuthal angle of 30° and a lessened flow separation range at 270° without the remarkable large vortices shedding in the wake of blade 3, which happens with the full blade. The boundary layer separation point delays from 0.7c with full blade to 0.967c for fixed flap slotted blade as shown in Table 5.

It is well known that the difference in pressure between the blade's upper and lower surface is the source of blade lift force and this constitutes an important part to the moment coefficient. Enhancement on the blade lift force can also increase the blade

Table 6
Summary of numerical cases for fixed flap.

	Slot angle (deg)	Slot width	Slot location	Flap angle (deg)
Slot angle effect	15	0.03c	0.7c	0
	30			
	60			
Slot width effect	30	0.02c	0.7c	0
		0.03c		
		0.04c		
Slot location effect	30	0.03c	0.6c	0
			0.7c	
			0.8c	
Flap angle effect	30	0.03c	0.7c	−30
				−15
				0
				15
				30

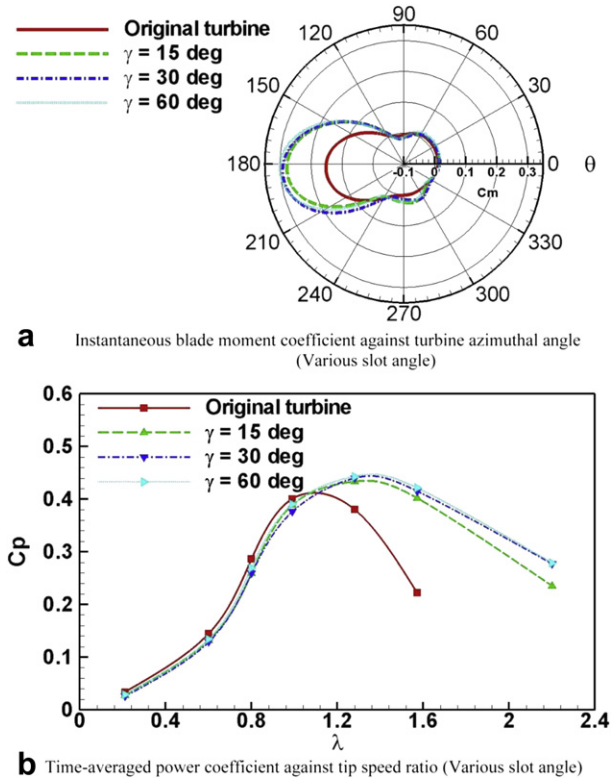

Fig. 13. Slot angle effect on instantaneous blade momentum coefficient and time-averaged power coefficient. ($w = 0.03c$, $L = 0.7c$ and $\beta = 0°$) (a) Instantaneous blade moment coefficient against turbine azimuthal angle; (b) Time-averaged power coefficient against tip speed ratio.

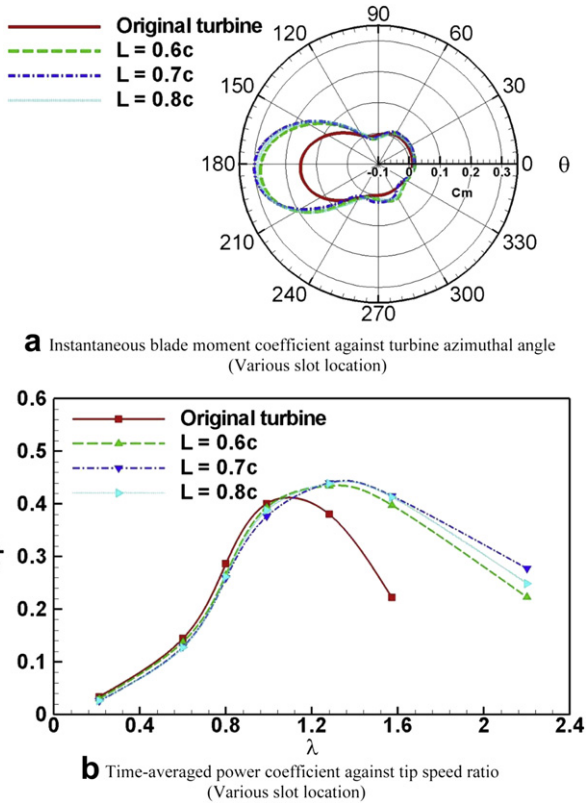

Fig. 15. Slot location effect on instantaneous blade momentum coefficient and time-averaged power coefficient. ($\gamma = 30°$, $w = 0.03c$, and $\beta = 0°$) (a) Instantaneous blade moment coefficient against turbine azimuthal angle; (b) Time-averaged power coefficient against tip speed ratio.

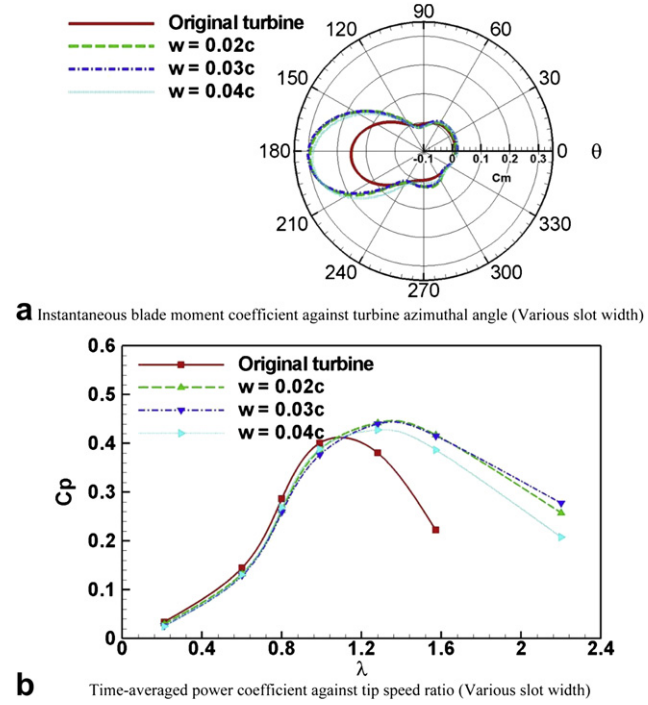

Fig. 14. Slot width effect on instantaneous blade momentum coefficient and time-averaged power coefficient. ($\lambda = 1.572$; $\gamma = 30°$; $L = 0.7c$) (a) Instantaneous blade moment coefficient against turbine azimuthal angle; (b) Time-averaged power coefficient against tip speed ratio.

torque relative to rotor, and the energy extraction capability of a lift-driven turbine. Fig. 11(a) and (b) compare the blade top and bottom wall pressure distribution for full and slotted blade associated with blade 1 and 3 shown in Fig. 10(a) and (b). It is seen that, a significant pressure difference between blade top and bottom walls occurs near the leading edge area, followed by a decreasing trend along blade surface. This is true for both full and slotted blades. However, a second peak occurs with a slotted blade near $x/c = 0.6–0.7$, which is attributed to the boundary layer re-development due to the slot. It is believed that such (second) peak plays a profound role on the increase of time-mean pressure difference for a slotted blade as compared to full blade. This is especially true when the blade rotates to the 270deg position.

We have discussed above the comparison between full blade and slotted blade with a fixed flap. A further investigation on the difference between a fixed flap and oscillating flap is carried out. The time-mean power coefficient shown in Table 5 indicates an improved energy extraction performance by using an oscillating flap. The increased instantaneous peak lift and momentum coefficients presented in Table 5 could be the reason for such an enhancement. Apart from this, further examination on the snapshots of instantaneous vortex contours within one revolution in Fig. 12 reveals some specific flow features.

Fig. 12(a)–(f) compare the vortex contour for the turbines with a slotted fixed and oscillating flap at three different azimuthal angles. It can be seen that, with a fixed flap, a long wake tail characterizing with a Karman vortices generates as the blades rotate, which results in a strong vortex interaction between two adjacent blades. This becomes more obvious when the blade locates at azimuthal angle of 90°. However, with an oscillating

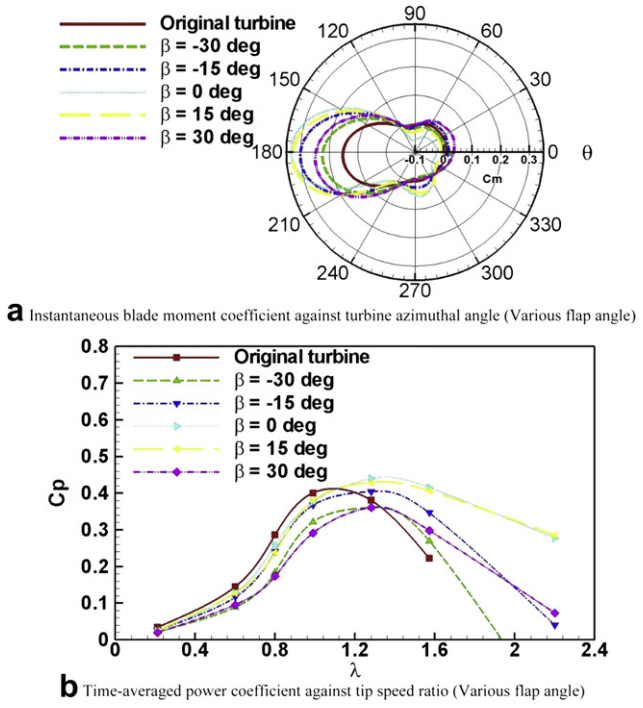

Fig. 16. Flap angle effect on instantaneous blade momentum coefficient and time-averaged power coefficient. ($\gamma = 30°$, $w = 0.03c$, and $L = 0.7c$) (a) Instantaneous blade moment coefficient against turbine azimuthal angle; (b) Time-averaged power coefficient against tip speed ratio.

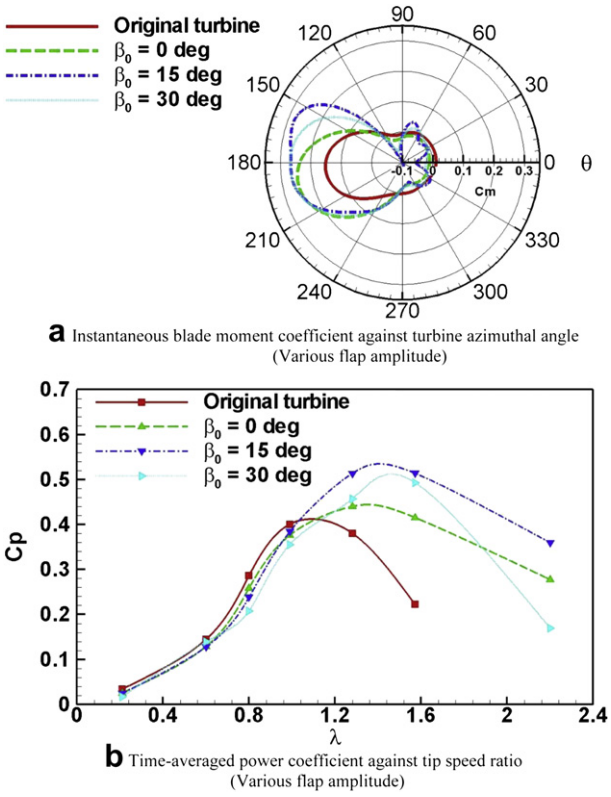

Fig. 17. Oscillating flap amplitude effect on instantaneous blade momentum coefficient and time-averaged power coefficient. ($\gamma = 30°$, $w = 0.03c$, $L = 0.7c$ and $n = 3$) (a) Instantaneous blade moment coefficient against turbine azimuthal angle; (b) Time-averaged power coefficient against tip speed ratio.

blade as shown in Fig. 12(d)–(f), the long wake tail is broken down by the periodic motion of oscillating flap, and vortex shedding from the upstream blade is quickly "thrown" away from wake leading to the weak vortex–blade interaction. This phenomenon is believed to suppress the top and bottom blade wall pressure difference declining trend, and ensure the blade lift force is sustained at a large level.

Based on above preliminary study on flow control mechanism from one specific case study, a systematic parametric study is further carried out with a series of variations on fixed and oscillating flap parameters. Computed results are presented in Section 3.3 for the fixed flap and 3.4 for the oscillating flap, respectively.

3.3. Slotted fixed flap parameters

Table 6 provides a summary of the main cases that are simulated in this section. These include a detailed investigation on the slot angle, width, location and fixed flap angle influences.

3.3.1. Slot angle

The investigation of slot angle effect is carried out for three different values, which are 15°, 30° and 60° at the slot width of 0.03c, slot location of 0.7c and flap angle of 0°. Fig. 13(a) shows the effect of slot angle on the instantaneous blade moment coefficient C_m. As seen from this figure, within an azimuthal angle from 0° to 60°, no apparent difference is observed on the blade moment coefficient for various blades studied here. A decreasing trend in C_m is shown within an azimuthal angle changing from 60° to 100°. Further increasing the azimuthal angle from 100° to 240°, a significant difference in C_m appears for full blade and slotted blade. The blade with 60° slot angle exhibits the largest peak C_m at about $\theta = 183°$, which is about twice of the peak C_m for full blade.

The comparison of various blades on the time-mean power coefficient variation with tip speed ratio is plotted in Fig. 13(b). As seen that, in comparison with full blade, the slotted blade covers a wider range of speed ratios at which the turbine remains as the largest power coefficient. The tip speed ratio to reach the peak power coefficient is also increased from $\lambda = 1.04$ to $\lambda = 1.36$. With regard to the low speed ratio range ($\lambda < 0.8$), the deviation among all blades could be neglected.

Above observations indicate that, the slot effect plays a significant role on the turbine performance at high speed ratios where the large boundary layer (BL) separation presents near the blade surface. Delaying this BL separation by using slot blade is therefore delaying the occurrence of dynamic stall to a higher speed ratio, and as a consequence leaving the turbine at a higher power extraction level within a much wider range speed ratio as compared to full blade.

Table 7
Summary of numerical cases for oscillating flap.

	Slot angle (deg)	Slot width	Slot location	Oscillating amplitude (deg)	Revolution ratio (n)
Oscillating flap amplitude effect	30	0.03c	0.7c	0 15 30	3
Revolution ratio effect	30	0.03c	0.7c	15	1 1.5 3

3.3.2. Slot width

The influence of slot width on the instantaneous moment coefficient is shown in Fig. 14(a). The general trend of C_m versus the

azimuthal angle (θ) curve is similar to that in Fig. 13(a), i.e., the apparent difference among full and slotted blade exists from $\theta = 120°–240°$ and minor discrepancy occurs between $\theta = 240°–330°$. The peak C_m jumps from 0.15 to 0.3 at $\theta = 180°$ when a slot is cut at 0.7 chord length from the leading edge. The comparison on various slot widths influence indicates that an intermediate width ($w = 0.03c$) is preferred in order to reach an optimal performance improvement. This is also well reflected from Fig. 14(b), where the time-averaged power coefficient against tip speed ratios is plotted. As it is seen from Fig. 14(b), the tip speed ratio to achieve the maximum power coefficient (C_p) extends from $\lambda = 1.04$ to $\lambda = 1.30$ if a slotted blade is used.

3.3.3. Slot location

From our previous discussion on the vortex contour in Section 3.2, it is known that the near wall blade boundary layer separation is well developed near 2/3 chord length. To control BL separation properly, the slot is expected to be cut around this area. The investigation on the slot location is performed for three slot positions of $L = 0.6c$, 0.7c and 0.8c. Fig. 15(a) shows the instantaneous blade moment coefficient against azimuthal angle (θ) for full blade and slotted blade with various slot locations. As expected, the blade with slot location of 0.7c obtains the largest C_m peak at the azimuthal angle of 180°, which is about twice of that obtained with full blade. The time-averaged power coefficients with different slot locations are compared in Fig. 15(b) along with full blade. It can be seen that, as compared to the turbine with full blades, the best slot location is observed at $L = 0.7c$, which increases the peak C_p from 0.4 to 0.45 and it also increases the speed ratio to attain this value as well.

3.3.4. Flap angle

With regard to the slot, apart from the slot angle, width and location discussed above, the flap angle is another important parameter as depicted in Fig. 1. A zero flap angle represents the fixed flap part being align with the main blade part without any bending. A positive flap angle represents the flap being bent towards to the lower side of the blade while a negative flap angle indicates the flap bent towards to the upper side of the blade. Five flap angles with β changing from $-30°$ to $+30°$ are investigated.

The comparison on the instantaneous momentum coefficient and time-mean power coefficient for various flap angles are plotted in Fig. 16(a) and (b), respectively. As seen from both figures, using a fixed flap generally increases the peck C_m at $\theta = 180°$ and extends the large power coefficient to a wider range of speed ratio. This is irrespective of whether the flap angle is positive, negative or zero. However, the best performance to enhance turbine energy extraction is achieved by using the flap with a zero angle. Bending flap either up or down relative to the blade front part diminishes the above improvement. This is expectable as the large flow separation occurs due to the sudden/sharp changing of blade surface streamline when the flap is bent up or down, which is similar to the classic back-step problem. Associated with this strong flow separation, the lift force will decrease and drag force will increase, leading to the decayed turbine performance. Such negative effect becomes more profound especially when turbine operates at low speed ratio

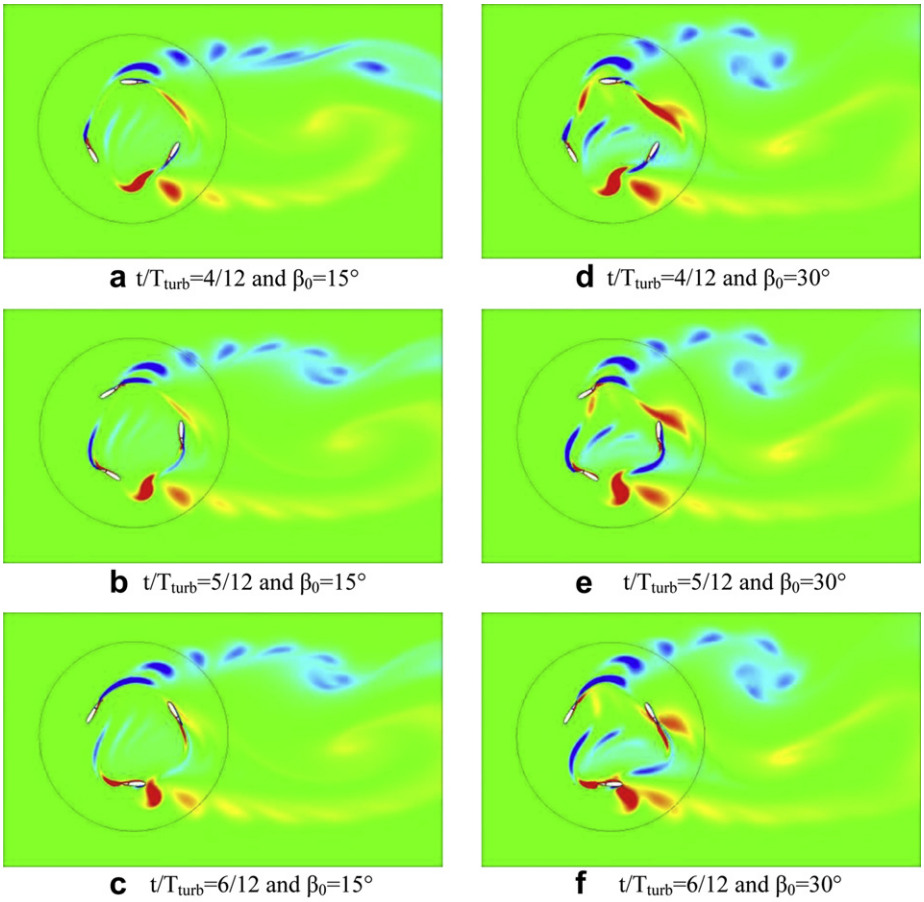

Fig. 18. Comparison of vortex contour for an oscillating flap blade with oscillating amplitude of $\beta_0 = 15°$ and $\beta_0 = 30°$ ($\lambda = 2.2$; $\gamma = 30°$; $w = 0.03c$; $L = 0.7c$; $n = 3$) (a) $t/T_{turb} = 4/12$ and $\beta_0 = 15°$; (b) $t/T_{turb} = 5/12$ and $\beta_0 = 15°$; (c) $t/T_{turb} = 6/12$ and $\beta_0 = 15°$; (d) $t/T_{turb} = 4/12$ and $\beta_0 = 30°$; (e) $t/T_{turb} = 5/12$ and $\beta_0 = 30°$; (f) $t/T_{turb} = 6/12$ and $\beta_0 = 30°$.

($\lambda < 1.2$). As displayed from Fig. 16(b), at a fixed speed ratio less than 1.2, adding fixed blade with a non-zero flap angle even worsens the turbine performance.

3.4. Oscillating flap parameters

The investigation of an oscillating flap influence on the turbine power performance is a further step study adopting the idea of slotted blade. The motion of the flap is defined in Eq. (1). As seen from the flap motion defined in Eq. (1), there are two parameters which influence the oscillating flap motion, i.e. the amplitude β_0 and the oscillating frequency, the latter is determined by the revolution ratio n. The study on the influence of flap motion on power extraction is therefore concentrated on these two parameters. Detailed information for various cases tested are summarized in Table 7.

3.4.1. Oscillating amplitude

The effect of oscillating amplitude on the instantaneous moment coefficient and time-mean power coefficient are shown in Fig. 17(a) and (b) for a comparison among the full blade, fixed flap blade ($\beta_0 = 0°$) and an oscillating flap blade ($\beta_0 \neq 0°$). It is evident that an oscillating flap enhances the turbine performance as compared to a fixed flap blade turbine or a full blade turbine. It can also be seen that the blade with the amplitude of 15° displays the widest large C_m region which covers the azimuthal angle from 145° to 200°. The high moment coefficient region becomes smaller when the flap oscillating amplitude increases from 15° to 30°. The maximum C_m of 0.28 is also achieved for a blade with the amplitude of 15°, which is about 12.98% times that of a blade with fixed flap. With regard to the time-mean power coefficient shown in Fig. 17(b), an increase of 23.72% C_p, as compared to fixed flap, is achievable with oscillating flap at 15° amplitude. As it is mentioned in Section 3.2, the flow control mechanism associated with an oscillating flap is related to the breakdown of vortex tail in the downstream wake of rotating blade. In addition, from our discussion on the flap angle effect in Section 3.3.4, it should also be noted that changing actual blade streamline via the use of fixed flap with non-zero flap angle is not beneficial to the boundary layer separation control. Using an oscillating flap resembles to adopting a flap with non-zero flap angle in terms of varying the actual blade streamline with a periodic motion. Therefore, to achieve a best performance, optimal oscillating amplitude is desired with which the vortex wake is properly broken down while the blade streamline is not significantly altered. A comparison on vortex contour for the oscillating flaps with amplitude of 15° and 30° are shown in Fig. 18(a)–(f). Clearly revealed from these figures that, the vortex interaction between two rotating blades becomes more chaotic and complicated with increasing oscillating amplitude from 15° to 30°, which is not an attractive feature in the search for a better performance turbine.

3.4.2. Oscillating frequency

The frequency of oscillating flap is another key parameter for the turbine with an oscillating flap blade. Based on Eqs. (1) and (2), the frequency is controlled by the revolution ratio n. There are three different revolution ratios tested in the present study which are 1.0, 1.5 and 3.0. Fig. 19(a) illustrates the instantaneous moment coefficient, which shows the differentiation on peak C_m for various oscillating frequency. The maximum C_m of 0.36 is observed when the flap oscillates at the same speed as that of blade rotating speed ($n = 1.0$). Increasing the flap revolution ratio from 1.0 to 1.5, the peak C_m and the width of the high C_m region remain the same but with an additional phase lag. Further increasing the flap revolution ratio from 1.5 to 3.0, the peak C_m drops while a slightly increased high C_m region is observable. In general, the effect of revolution ratio (n) on the C_m distribution and magnitude could be ignored. This is also indicated from Fig. 19(b) where the time-mean power coefficients are compared for fixed flap, oscillating flap with varying n and full blade.

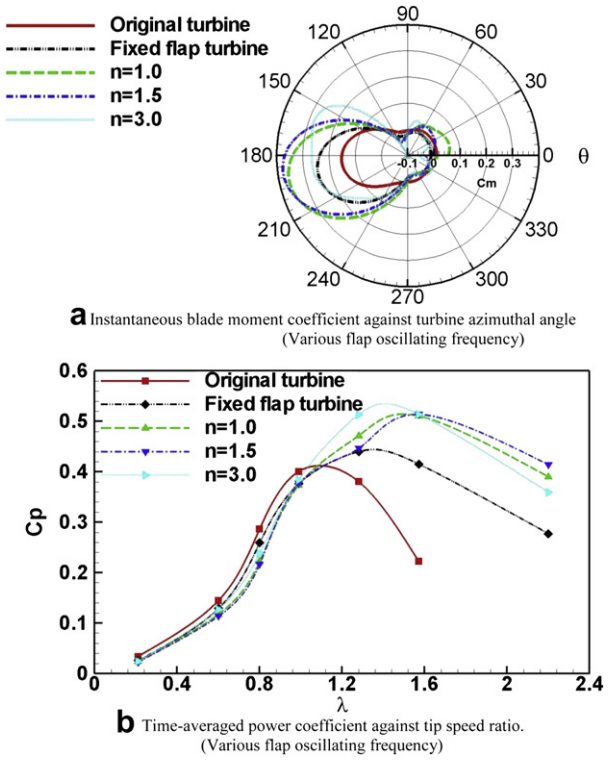

Fig. 19. Oscillating flap frequency effect on instantaneous blade momentum coefficient and time-averaged power coefficient. ($\gamma = 30°$, $w = 0.03c$, $L = 0.7c$ and $\beta_0 = 15°$) (a) Instantaneous blade moment coefficient against turbine azimuthal angle; (b) Time-averaged power coefficient against tip speed ratio.

4. Conclusions

In this study, a new concept via the use of a fixed and oscillating flap to moderate the traditional H-shaped VATT blade is proposed. By a systematic numerical modeling investigation, the potential benefit to improve the VATT energy extraction efficiency is explored. Simulation results indicate that the fixed and oscillating flap techniques indeed enhance the VATT performance significantly, especially at large tip speed ratio, where the boundary layer separation dominates the flow. In addition, it is found that an oscillating flap presents a better performance than that of a fixed flap. The parametric study performed provides the optimal geometry parameters under the real operating conditions. For a fixed flap blade, these include a slot angle of 60°, slot width of 0.03c, slot location at 0.7c. With an oscillating flap, additional parameters include the oscillating amplitude of 15° and the revolution ratio of 1.5. With the above parameters, the peak power coefficient (C_p) rises about 28% relative to the full blade turbine and the thread shed of tip speed ratio at which the C_p exhibits decaying trend increases about 43% as well. Examination on the flow details around the rotating blade indicates that the dynamic stall associated with turbine blade at large AOA is effectively delayed with the use of fixed blade. With an oscillating flap, it provides one additional influence on reducing the blade wake vortex interaction. Both of the above two factors are beneficial in order to increase the blade lift coefficient, momentum coefficient and thus the overall efficiency of turbine.

Acknowledgments

We are grateful to the High Performance Computer (HPC) at University of Strathclyde for partial support of this work.

References

[1] Nicholls-Lee RF, Turnock SR, Boyd SW. Simulation based optimization of marine current turbine blades. 7th International Conference on Computer and IT Applications in the Maritime Industries (COMPIT'08), Liège, Belgium; 21–23 Apr. 2008.
[2] Gretton GI, Bruce T, Ingram DM. Hydrodynamic modeling of a vertical axis tidal current turbine using CFD. 8th European Wave and Tidal Energy Conference, Uppsala, Sweden; 2009.
[3] Gretton GI. The hydrodynamic analysis of a vertical axis tidal current turbine. Ph.D thesis, University of Edinburgh; 2009.
[4] Page H. The handley page wing. Aeronautical Journal 1921:263–89.
[5] Glauert H. The handley page slotted wing. London, R&M No. 834: Aeronautical Research Council; Mar. 1922.
[6] Weyl AR. High-lift devices and tailless aeroplanes. Aircraft Engineering and Aerospace Technology 1945;17(11):325–30.
[7] Fowler HD. Variable lift. Western flying; November, 1931. p. 31–3.
[8] Weick FE, Platt RC. Wind-tunnel tests of the fowler variable-area wing. National Advisory Committee for Aeronautics; May, 1932. No. 419.
[9] Smith A. High-lift aerodynamics. Vol. 12, No. 6, AIAA 6th aircraft design, flight test and operations meeting, Los Angeles, Calif.; August 12–14, 1974.
[10] Dam CV. The aerodynamic design of multi-element high-lift systems for transport airplanes. Progress in Aerospace Sciences 2002;38:101–44.
[11] Reckzeh D. Aerodynamic design of the high-lift-wing for a mega liner aircraft. Aerospace Science and Technology 2003;7:107–19.
[12] Xiao Q, Liao W. Numerical investigation of angle of attack profile on propulsion performance of an oscillating foil. Computers and Fluids 2010;39:1366–80.
[13] Xiao Q, Liao W, Yang SC. How motion trajectory affects the energy extraction performance of an oscillating foil. Renewable Energy 2012;37:61–75.
[14] Sun K, Zhang L, Shao W, Zhou P. Numerical simulating method for passive control vertical turbine in marine stream energy. GreenTech-international conference on marine science & technology for green shipping; 17th–18th June 2009.
[15] Castelli MR, Englaro A, Benini E. The Darrieus wind turbine: proposal for a new performance prediction model based on CFD. Energy 2011;36:4919–34.